70th International Astronautical Congress (IAC), Washington D.C., United States, 21-25 October 2019.

IAC-19,A7,3,4,x50556

Imaging Terrestrial Extrasolar Planets using Submicron Interferometric Platforms

Collins Ogundipe[a], Alex Ellery[a]*

[a] *Space Exploration and Engineering Group, Carleton University, Canada,* aellery@mae.carleton.ca
* Corresponding Author

Abstract

A technique based on the employment of a suite of onboard manipulators has been used to automatically adjust the configuration of free-flying telescopes, in order to maintain the constellation as a virtual optical bench. The goal was to simulate a sufficiently stable and accurate platforms for interferometric imaging. A mapping algorithm has been developed demonstrating the relationship between the robotic manipulators' configuration such that joint-level trajectories are deduced to move or re-position the robotic arm, resulting in a successful approach to accurately control the relative spacing between the interferometric platforms. Each interferometric platform represents a spacecraft bus mount to which one or more manipulators are mounted. No fuel is expended except for the initial configuration maneuvers. The imaging resolution of Proxima Centauri b was assessed and the types of features that could be detected.

Keywords: extrasolar planet, interferometric, robotic manipulator, resolution, constellation, telescope.

1. Introduction

Direct imaging of extrasolar planets is the holy grail of extrasolar planet exploration. Although current astronomical techniques are improving in leaps and bounds, systematic direct imaging of extrasolar planets, particularly terrestrial-type planets, has not yet been possible. Previous proposals such as the European Darwin interferometer faltered on the lack of technological maturity at the time. A technique is hereby introduced that permits the control of relative position of a Darwin-type constellation to submicron/micron accuracies. With submicron relative positioning accuracy, interferometric methods offer extremely high-resolution imaging. With the implementation of near-infrared interferometric constellations, free-flying telescopes can combine into a 'virtual telescope' with a much larger diameter represented by the utmost-separated apertures. The idea introduced here is to use the robotic manipulator's movement to control the base reactions and translational motion at the spacecraft platform. The path and motion of the robotic arm has been mapped to dictate the coupling reaction effect at the spacecraft platform [1]. The benefit of this is that, for such relative fine positioning movement, no fuel or traditional ion engine technology is utilized or required in space. This approach is explored here in the study of interferometric imaging of terrestrial extrasolar planets, using a constellation of space robots (telescopes) acting in formation flying as stable and accurate optical bench. The aim is to control the position of the space telescopes such that their center of mass remains invariant relative to one another, in the event of perturbation and disturbance.

2. Astronomical Optics

In classical (physical) optics, light is propagated as a wave. The speed of light wave in air is given as 3.0×10^8 m/s approximately. The wavelength of visible light waves varies between 400 nm and 700 nm, but the term "light" is often used for near-infrared as well (wavelength above 700 nm to 1 mm). The wave model can be used to infer how an optical system will behave without requiring an explanation of what is transmitting in the medium.

For different light sources, there are factors that limit the ability of an optical aperture (or detector) to optically resolve an image. One of such is the diffraction effects. In general, light that is passing through an aperture will experience diffraction. According to diffraction-limited optics, the best images that can be created will appear as a central spot with surrounding bright rings in a pattern known as the Airy pattern, and the central bright lobe referred to as the Airy disk. The size of the airy disk is given by $\theta = 1.22\frac{\lambda}{D}$, where θ is the angular resolution, λ is the wavelength of the light, and D is the diameter of the lens aperture. In physical optics, if the angular separation of two points is significantly less than the Airy disk angular radius, then the two points cannot be

resolved in the image. Going by the Rayleigh criterion, it is stipulated that two points whose angular separation is equal to the Airy disk radius measured to first null (the first place where no light is seen) can be taken as fully resolved. With this, it can be deduced that the greater the diameter of the lens or its aperture, the finer the resolution. This brings us to the importance of interferometry, and why we have adopted interferometric platforms in this study. Interferometry, with its ability to mimic extremely large baseline apertures, allows for greater lens diameter, and hence offers the possibility for much greater angular resolution. For astronomical imaging, the atmosphere prevents optimal resolution from being achieved in the visible (light) spectrum due to scattering and dispersion. Hence, the infrared spectrum was adopted for this study to reduce disruption of images and achieve results that approach the diffraction limit. Conversely, the infrared offered us a much greater wavelength to achieve a required angular resolution up to 1 milliarcseconds needed to resolve the Proxima Centauri, for instance, using an aperture of 250 m diameter in a single pixel.

In physical optics, the process involved in setting tolerances begins with setting of the minimum level of acceptable image quality. This is usually expressed as the desired level of contrast at a specific spatial frequency as expressed by the modulation transfer function (MTF). The modulation transfer function is one of the main criteria for judging the image quality of an imaging system. Together with the well-known optical transfer function, the MTF can be regarded as an optical bench measurement used to evaluate the performance of a lens, or a lens system. Hence, the MTF is regarded as an objective basis reflecting the comprehensive performance of an imaging interferometer. In this study as it applies to free-formation flying of telescopes serving as interferometric platforms, the accuracy and precision of the separation distance between the optical/interferometric bench is a major factor in actualizing MTF and image quality; much like the case of keeping a fixed focal length, and precise diameter of the lens (aperture) to a submicron accuracy, so as to achieve the best modulation transfer function. Modulation is a ratio of image contrast to object contrast. Ideally, it would be one, or 100%. Similar studies have been carried out (or attempted) in the past. One is the suspended European Space Agency (ESA) Darwin mission which would have involved a constellation of four to nine spacecraft designed to directly detect Earth-like planets orbiting nearby stars and search for evidence of life on these planets. The proposed design envisaged three free-flying space telescopes, each three to four metres in diameter, flying in formation as an astronomical interferometer. A fourth spacecraft would have contained the beam combiner, spectrometers, and cameras for the interferometer array. Another similar mission to Darwin was the NASA Terrestrial Planet Finder (TPF) which was a proposed project to construct a system of space telescopes for detecting extrasolar terrestrial planets. TPF was postponed several times and indefinitely suspended in 2011 by the US Senate due to spending limit and lack of fund. This paper has shown that this concept can be brought back (revived) in a more achievable and cost-effective approach. Similar to TPF, the approach proposed in this study involved infrared astronomical interferometer with multiple (4 or 5) small telescopes on separated spacecraft floating in precision formation simulating a much larger, very powerful telescope. It has been shown that robotic manipulators on board the telescopes can be used to maintain precision formation, which is the key to achieving high resolution image quality.

3. Constellation Theory

The main approach adopted in this study is based on a mission that would involve a constellation of five spacecraft (telescopes) along with another separate spacecraft at the centre acting as the beam combiner and spectrometer. This constellation is similar in approach to ESA's Darwin and NASA's TPF proposed to directly detect Earth-like planets orbiting nearby stars and search for evidence of life on these planets – using the method of astronomical interferometer. Astronomical interferometer is an array of separate telescopes or mirror segments that work together as a single telescope to provide higher resolution images of astronomical objects such as stars and exoplanets by means of interferometry. The advantage of this technique is that it can theoretically produce images with the angular resolution of a huge telescope with an aperture equal to the separation between the component telescopes. The main drawback is that it does not collect as much light as the singular instrument's mirror. Thus, it is mainly useful for fine resolution of more luminous astronomical objects, like binary stars and triple star systems such as Beta Centauri, Alpha Centauri A-B and stars in the southern constellation of Centaurus. Another drawback is that the maximum angular size of a detectable emission source is limited by the minimum gap between detectors in the collector array [2].

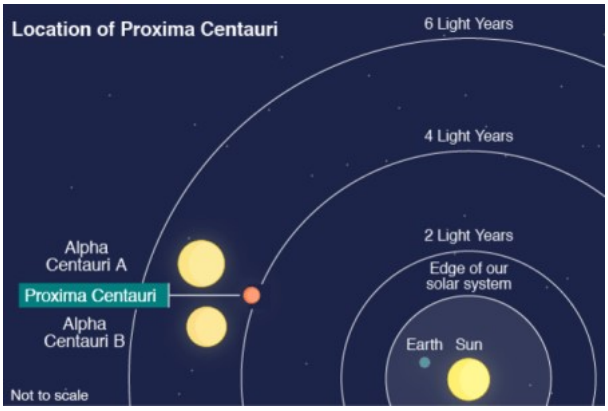

Fig. 1. Proxima Centauri location in comparison to Earth/Sun [3].

Although Proxima Centauri (Alpha Centauri C) has a very low average luminosity, Proxima is a flare star that undergoes random dramatic increases in brightness because of magnetic activity [4]. The star's magnetic field is created by convection throughout the stellar body, and the resulting flare activity generates a total X-ray emission similar to that produced by the Sun. At the shorter wavelengths used in infrared astronomy and optical astronomy, it is more difficult to combine the light from separate telescopes, because the light must be kept coherent within a fraction of a wavelength over long optical paths, requiring very precise optics. Robotic manipulators can be explored to maintain this precision as required between the separated telescopes up to submicron accuracy. Once precision and accuracy can be guaranteed (as would be necessary during perturbation), then astronomical interferometers can produce higher resolution astronomical images than any other type of telescope. The approximate angular diameter (resolution) of any planet is given by $\delta = 2\ arctan(d/2D)$, where d is the diameter of the planet, and D is the distance of the imaging constellation to the exoplanet. For Proxima Centuari, we will assume the constellation is just at Low-Earth orbit, simply using the approximate distance to the Sun (since the distance between low-Earth and the sun is quite insignificant compared to the Proxima distance to the Sun). Therefore, D, will be taken as approximately 4.2 light years (41.3×10^{12} Km); diameter (d) of Proxima is 214,550 Km. Hence,

$$\delta = 2\ arctan\left(\frac{214{,}550}{2 \times (41.3 \times 10^{12})}\right)$$

$$\delta = 2.98 \times 10^{-7^\circ}$$

$$= 0.001 \text{ arcseconds } (1 \text{ milliarcseconds})$$

As discussed in Section 2, image resolutions of a fractional milliarcseconds can been achieved at infrared wavelengths. Using the angular resolution (θ) formula of diffraction limit (Airy disk),

$$\theta = 1.22\left(\frac{\lambda}{D}\right), \quad (1)$$

Using an infrared wavelength of about 1065 nm and interferometric bench separation of 250 m aperture diameter,

$$\theta = 1.22\left(\frac{1065 \times 10^{-9}}{250}\right)$$

$$= 5.2 \times 10^{-9} \text{ radians } (2.98 \times 10^{-7^\circ})$$

$$= 0.001 \text{ arcseconds } (1 \text{ milliarcseconds})$$

The angular resolution (θ) of 1 milliarcseconds as gotten would have been sufficient to resolve the Proxima Centuari, with an infrared wavelength of about 1065 nm. The simple layout of an astronomical interferometer could be such of a pentagonal or rectangular arrangement of separated telescopes, giving a partially complete reflecting telescope, but with the need to ensure that the optical path lengths from the astronomical object to the beam combiner (focus) are the same as would be required by a complete (single) telescope case.

4. Kinematics Analysis of Space-based Manipulator

To control the positioning of space telescopes (spacecrafts), free-flying systems in which one or more manipulators are mounted on the spacecrafts have been explored. In this mode of operation, the attitude control is achieved by the reaction wheels and the spacecrafts are allowed to translate in response to their manipulators' motions. Therefore, non-zero momentum are eliminated in the system. Reaction wheels (also called momentum wheels) are usually mounted on three orthogonal axes aboard the spacecraft. This study detailed the application of robotic manipulators for translational movement of the spacecraft such that the relative distance between a constellation of free-flying spacecrafts can be controlled. The primary differentiating characteristics of space robotics from terrestrial robotics is that the robot operates in a microgravity environment. The environmental disturbance torques (gravity gradient, aerodynamics and magnetic torques) imposed on the robot spacecraft are very small – within 10e-6 Nm [5]. While terrestrial robots are mounted onto a firm ground, in space, there is no such reaction force or torque cancellation to the motion of the robotic arms. This will induce translational motion on the satellite platform in response to the movement of the manipulator.

In the consideration of a free-flying robotic manipulator with dedicated attitude control of the spacecraft bus, the

position kinematics of the space manipulator with respect to inertial space could be represented by [6, 7]

$$p^* = r_{c0} + R_0 s_0 + \sum_{i=1}^{n} R_i\, l_i \qquad (2)$$

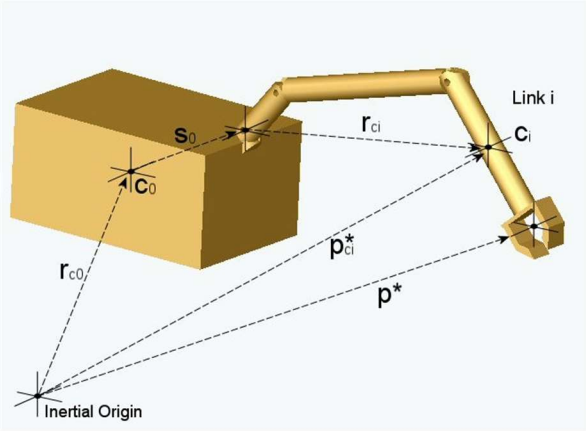

Fig. 1. Spacecraft-Manipulator Geometry

For an attitude-controlled platform, $R_0 = I_3$ (identity matrix). The center of mass of the complete system (the satellite bus mount, robotic manipulator and the payload) is given by [6, 7]

$$p^*_{cm} = \frac{\sum_{i=0}^{n+1} m_i\, p^*_{ci}}{\sum_{i=0}^{n+1} m_i} \qquad (3)$$

where p^*_{cm} is the location of the centre of mass of the entire robot/spacecraft system with respect to the inertial coordinates; m_i is the mass of each component rigid body links; n is the number of serial rigid body links; $n = 0$ is the link representing the spacecraft body; i link number from 0 to n; p^*_{ci} is the position of link i centre of mass with respect to the inertial coordinates; As it is for the case of terrestrial manipulator, it is equally necessary to find the location of the system centre of mass with respect to inertial coordinates (origin) where it remains invariant [6]. If no external forces act on the system, the location of the centre of mass will remain invariant in inertial space;

$$\sum_{i=0}^{n+1} F_i = \sum_{i=0}^{n+1} m_i\, \ddot{p}^*_{ci} = 0, \text{ such that } p^*_{cm} = 0 \qquad (4)$$

This will correspond to the 'inertial ground' defined of an ideal kinematic chain [8, 9]. The inertial (virtual) ground is the point in inertial space at which an ideal virtual kinematic chain manipulator has its base. The virtual ground point coincides with the centre of mass of the spacecraft-manipulator system. The system centre of mass is the point at which all the mass may be considered to be concentrated. Then,

$$p^*_{ci} = \sum_{j=0}^{i} r_{cj}$$

Substitution of the above into equation (2) yields

$$p^*_{cm} = \frac{1}{m_T}\left(\sum_{i=0}^{n+1} m_i \sum_{j=0}^{i} r_{cj}\right) = \frac{1}{m_T}\left(\sum_{i=0}^{n+1}\sum_{j=i}^{n+i} m_j\, r_{ci}\right)$$
$$= r_{c0} + \frac{1}{m_T}\sum_{i=1}^{n+1}\sum_{j=i}^{n+i} m_j\, r_{ci} \qquad (5)$$

Now, the vector of the centre of mass of each link and the vectoral length of each link are defined as

$$r_{ci} = R_i r_i + R_{i-1} s_{i-1}$$
$$l_i = r_i + s_i \qquad (6)$$

These definitions are then substituted into equation (4)

$$p^*_{cm} = r_{c0} + \frac{1}{m_T}\sum_{i=1}^{n+1}\sum_{j=1}^{n+1} m_j\, R_{i-1}(r_{i-1} + s_{i-1})$$
$$+ \frac{1}{m_T}\sum_{i=1}^{n+1} m\, R_i r_i$$
$$= r_{c0} + \frac{1}{m_T}\sum_{i=1}^{n+1}\sum_{j=i}^{n+i} m_j\, R_{i-1} l_{i-1} + \frac{1}{m_T}\sum_{i=1}^{n+1} m\, R_i r_i \qquad (7)$$

The equation (6) was restructured to match the terrestrial manipulator algorithms of the form: $p_i = R_i l_i$, then we have [2]

$$p^*_{cm} = r_{c0} + (1 - \frac{m_0}{m_T}) s_0 + \frac{1}{m_T}\sum_{i=1}^{n} R_i \left(\sum_{j=i+1}^{n+1} m_j\, l_i + m_i r_i\right)$$
$$+ \frac{m_{n+1}}{m_T} R_{n+1} r_{n+1}$$

This above equation has been separated out into three components: components associated with body 0 (the spacecraft), bodies 1 to n (the manipulator links) and body $n + 1$ (the payload). This then reduces to

$$p^*_{cm} = r_{c0} + (1 - \frac{m_0}{m_T}) s_0 + \sum_{i=1}^{n} R_i\, L_i + (\frac{m_{n+1}}{m_T}) r_{n+1}$$
$$\text{where } L_i = \frac{1}{m_T}\left(\sum_{j=i+1}^{n+1} m_j\, l_i + m_i r_i\right) \qquad (8)$$

This completes the location of the center of mass of the system with respect to inertial space. It is assumed arbitrarily that the local inertial reference frame initially coincides with the spacecraft bus center of mass, that is, $r_{c0} = 0$, since any point fixed in the interceptor body may be regarded as inertially fixed prior to any robotic maneuver [10]. To continue the generalized formulation, r_{c0} is then substituted into equation (1), having defined p^*_{cm};

$$p^* = p^*_{cm} + s_0 + \sum_{i=1}^{n} R_i\, l_i - \frac{1}{m_T}\sum_{i=1}^{n+1}\sum_{j=i}^{n+1} m_j\, r_{ci} \quad (9)$$

Similar to the procedure employed earlier for equation (4), the equation (5) is then substituted into equation (8);

$$p^* = p^*_{cm} + s_0 + \sum_{i=1}^{n} R_i\, l_i - \frac{1}{m_T}\sum_{i=1}^{n+1}\sum_{j=i}^{n+1} m_j\,(R_i r_i + R_{i-1} s_{i-1}) \quad (10)$$

An attempt was then made to separate out the components relating to the spacecraft mounting (body 0), the manipulator links (bodies 1 to n) and the payload (body n + 1) [2]. This gives

$$p^* = p^*_{cm} + \frac{m_0}{m_T} s_0 + \sum_{i=1}^{n} R_i\, \lambda_i - \frac{m_{n+1}}{m_T} R_{n+1} r_{n+1}$$

$$\text{where } \lambda_i = \frac{1}{m_T}\sum_{j=0}^{i} (m_j l_j - m_i r_i) \quad (11)$$

Accordingly, λ_i is referred to as the lumped kinematic parameter for each manipulator link. This above equation of p^* has the same form as that of Earth-based manipulator of the form $p = \sum_{i=1}^{n} R_i\, l_i$ with additional constants (p^*_{cm} is constant, and λ_i is constant as the lumped kinematic/dynamic parameter, replacing the l_i in earth-based manipulator).

5. Resolved Motion Control

Resolved motion control commands the manipulator hand to move in a desired cartesian direction in a coordinated position and rate control; meaning the motions of the various joint motors are combined and resolved into separately controllable hand motions along the world coordinates axes. The kinematics of robotic manipulators are defined such that at each joint i a reference frame is assigned to form a sequence of coordinates from the base (joint $i = 0$) to the end-effector (joint $i = n$). The Denavit-Hartenberg (DH) 4 X 4 matrix formulation for manipulator kinematics is well developed and widely used in robotics [11, 12, 13]. The DH matrix connect each sequential coordinate frame from the base ($i = 0$) to the end-effector ($i = n$) to provide the basis for relating joint angles to the cartesian position of the end-effector as a sequence of rigid body motion [14]. The DH matrix formulation expresses the geometry of space manipulator as a non-linear mapping given by [14, 15]

$$[q] = \begin{bmatrix} n & s & a & p^* \\ 0 & 0 & 0 & 1 \end{bmatrix} = \begin{bmatrix} R & p^* \\ 0 & 1 \end{bmatrix}$$

where R is a 3 x 3 direction cosine matrix represented as (nsa) as for terrestrial manipulators, and p^* is as defined in equation (10). The $q = (nsap)$ is the generalized Cartesian position of the end-effector with respect to the base coordinates; n is the normal vector; s is the slide vector parallel to the end-effector finger grip, a is the approach vector; and p is the cartesian position vector of the end-effector with respect to the base coordinates. The same algorithms based on the DH matrix used for terrestrial manipulators can be used for computing the position of the end-effector of the robot in the inertial space. This makes it possible to compute the inverse kinematics problem of determining the joint angles of the position in the Cartesian coordinates for resolved motion control. Therefore, the inverse kinematics solution to the manipulator geometry can be found with little modifications to the terrestrial algorithms. Calculation of end-effector velocity involves the use of Jacobians (matrix) which relates the end-effector's velocity to joint angle rates. For a free-flying robotic manipulator employing attitude control, the manipulator Jacobian matrix is given by [14, 15]

$$\bar{J} = \sum_{i=1}^{n}\sum_{k=1}^{i} \frac{\partial R_i}{\partial \theta_k}\lambda_i \quad (12)$$

where R_i and λ_i are same as represented in equation (10); θ represents the joint angles. The space manipulator Jacobian requires only the replacement of kinematic link parameters with those of the kinematic-dynamic parameters (λ_i), and the positional constrains differenciated to zero. Therefore, the Jacobian maybe inverted as normally done for the terrestrial manipulators. The Jacobian matrix could also be calculated as the by-product of the Newton-Euler dynamic analysis through the vectoral representation of the velocities and angular velocities of each manipulator link [16]. From the Jacobian matrix, it is equally possible to compute resolution of acceleration between the end-effector and the manipulator joints in the form $\ddot{q} = J\ddot{\theta} + \dot{J}\dot{\theta}$ [17].

6. Space Manipulator Dynamics and Controller

For a space manipulator with multiple joints, one of the basic control schemes that has been recommended is the computed torque technique based on the Lagrange-Euler (L-E) or Newton-Euler (N-E) dynamics - equations of motion [18]. However, the N-E method remains far more efficient than the recursive L-E method, and for this reason was adopted for dynamic simulation of most space manipulators. Several dynamic formulations for multi-body space systems have been subjected to comparison, and these studies concluded that the recursive N-E methods are much more efficient computationally than the L-E approaches [19], a conclusion reiterated in its application to space-based

manipulators [20]. The Newton-Euler equations of motion consist of a set of forward and backward recursive equations. These equations are:

Forward recursive equations: $i = 1, 2, \ldots, n$

$$\omega_i = \begin{cases} \omega_{i-1} + z_{i-1}\dot{q}_i & \text{if link } i \text{ is rotational} \\ \omega_{i-1} & \text{if link } i \text{ is translational} \end{cases}$$

$$\dot{\omega}_i = \begin{cases} \dot{\omega}_{i-1} + z_{i-1}\ddot{q}_i + \omega_{i-1} \times (z_{i-1}\dot{q}_i) & \\ \quad \text{if link } i \text{ is rotational} & \\ \dot{\omega}_{i-1} \quad \text{if link } i \text{ is translational} & \end{cases}$$

$$\dot{v}_i = \begin{cases} \dot{\omega}_i \times p_i + \omega_i \times (\omega_i \times p_i) + \dot{v}_{i-1} & \\ \quad \text{if link } i \text{ is rotational} & \\ z_{i-1}\ddot{q}_i + \dot{\omega}_i \times p_i + 2\omega_i \times (z_{i-1}\dot{q}_i) \; + & \\ \omega_i \times (\omega_i \times p_i) + \dot{v}_{i-1} & \\ \quad \text{if link } i \text{ is translational} & \end{cases}$$

$$\overline{v}_i = \omega_i \times \overline{s}_i + v_i$$

$$\overline{a}_i = \dot{\omega}_i \times \overline{s}_i + \omega_i \times (\omega_i \times \overline{s}_i) + \dot{v}_i$$

Backward recursive equations: $i = n, n\text{-}1, \ldots, 1$

$$F_i = m_i \overline{a}_i$$

$$N_i = I_i \dot{\omega}_i + \omega_i \times (I_i \omega_i)$$

$$f_i = F_i + f_{i+1}$$

$$n_i = n_{i+1} + p_i \times f_{i+1} + (p_i + \overline{s}_i) \times F_i + N_i$$

$$\tau_i = \begin{cases} n_i^T z_{i-1} + b_i \dot{q}_i & \text{if link } i \text{ is rotational} \\ f_i^T z_{i-1} + b_i \dot{q}_i & \text{if link } i \text{ is translational} \end{cases}$$

where b_i is the viscous damping coefficient for joint i; m_i is the total mass of link i; $\overline{s}_i$ is the position of the center of mass of link i from the origin of the coordinate system (x_i, y_i, z_i); p_i is the origin of the ith coordinate frame with respect to the $(i-1)$th coordinate frame; $\overline{r}_i$ is the position of the center of mass of link i from the origin of the base reference frame; $\overline{v}_i$ is the linear velocity of the center of mass of link i $(d\overline{r}_i/dt)$; $\overline{a}_i$ is the linear acceleration of the center of mass of link i $(d\overline{v}_i/dt)$; F_i is the total external force exerted on link i at the center of mass; N_i is the total external moment exerted on link i at the center of mass; I_i is the inertia matrix of link i about its center of mass with reference to the coordinates system (x_0, y_0, z_0); f_i is the force exerted on link i by link $i-1$ at the coordinate frame $(x_{i-1}, y_{i-1}, z_{i-1})$ to support link i and the links above it; n_i is the moment exerted on link i by link $i-1$ at the coordinate frame $(x_{i-1}, y_{i-1}, z_{i-1})$. The recursive equations were implemented with respect to individual link about its own coordinate frame, such that we have forward recursive equations as:

$$^{i}R_0\omega_i = \begin{cases} ^{i}R_{i-1}(^{i-1}R_0\omega_{i-1} + z_0\dot{q}_i) & \\ \text{if link } i \text{ is rotational} & \\ ^{i}R_{i-1}(^{i-1}R_0\omega_{i-1}) \quad \text{if link } i \text{ is translational} & \end{cases}$$

$$^{i}R_0\dot{\omega}_i = \begin{cases} ^{i}R_{i-1}[^{i-1}R_0\dot{\omega}_{i-1} + z_0\ddot{q}_i + (^{i-1}R_0\omega_{i-1}) \times & \\ z_0\dot{q}_i] \text{ if link } i \text{ is rotational} & \\ ^{i}R_{i-1}(^{i-1}R_0\dot{\omega}_{i-1}) \quad \text{if link } i \text{ is translational} & \end{cases}$$

$$^{i}R_0\overline{v}_i = R_0(\omega_i \times \overline{s}_i + v_i) \ldots \text{and so on}$$

The steps were completed for all the forward and backward recursive equations for link-based (each link's own coordinate).

Under the computed torque control law implemented for the controller of the multi-joint space manipulator, the comparative control law in the joint-variable space has been derived from the N-E equations of motion [16]. The control law is computed recursively, and the resulting control law can be obtained by substituting $\ddot{q}_i(t)$ into the N-E equations to obtain the necessary joint torque for each actuator:

$$\ddot{q}_i(t) = \ddot{q}_i^d(t) + \sum_{j=1}^{n} K_v^{ij}\,[\dot{q}_j^d(t) - \dot{q}_j(t)] + \sum_{j=1}^{n} K_p^{ij}\,[q_j^d(t) - q_j(t)] \qquad (13)$$

where K_v^{ij} and K_p^{ij} are the derivative (velocity) and position feedback gains for joint i respectively and $e_j(t) = q_j^d(t) - q_j(t)$ is the position error for joint j. The physical meaning of putting the equation (12) into the N-E recursive equations can be interpreted that the first term will generate the desired torque for each joint if there is no modelling error and the physical system parameters are known [16]. The remaining terms will generate the correction torque to compensate for the deviations from the desired joint trajectory. The recursive control law is a proportional plus derivative (PD) control law and has the effect of compensating for inertial loading and coupling effects of the links; there is no gravity loading. The computed control law is a linearized feedforward model-based PD feedback control system based on inverse dynamics.

7. Simulations and Results

7A. Simulation - Stabilization of a Single Platform

To demonstrate the use of the robotic manipulator in keeping the optical bench stable, a single platform space robot has been simulated. Figure 1 as shown in section 4 is a representation of a single robot-spacecraft system. Recall equation (8) in section 4 where the robot-spacecraft center of mass (p_{cm}^*) was given by:

$$p_{cm}^* = r_{c0} + (1 - \frac{m_0}{m_T})s_0 + \sum_{i=1}^{n} R_i\,L_i + (\frac{m_{n+1}}{m_T})r_{n+1}$$

$$\text{where } L_i = \frac{1}{m_T}(\sum_{j=i+1}^{n+1} m_j\,l_i + m_i r_i)$$

It can be deduced that the system center of mass with respect to the inertial space is determined by vector r_{c0} from the inertial origin to the spacecraft center of mass

and the fixed lever arm distance s_0 from the spacecraft center of mass to the base of the robotic manipulator. Since the lever arm distance (s_0) would always be fixed and the link masses would always be predetermined, the parameter r_{c0} provides a way to manipulate and adjust the position of the spacecraft center of mass. If an algorithm could be developed to keep r_{c0} stable or adjustable, it means the center of mass of the spacecraft can be kept at a desired position in relation to another fixed reference (for example, another stable spacecraft platform). It has been shown that the movement of the robotic arm directly induces a reaction force on the spacecraft at the manipulator base, thereby changing the position of the vector r_{c0} [10]. In such instance, in order to find the system center of mass with respect to inertial space, it is first assumed arbitrarily that the local inertial reference frame initially coincides with the center of mass of the spacecraft bus, that is, r_{c0} = 0, – since any point fixed in the interceptor body may be regarded as inertially fixed prior to any robotic maneuver. With r_{c0} taken as zero, to find p^*_{cm}, initialization may be performed for any arbitrary robot configuration, e.g. 'tucked' (stowed) position – by implementing equation (7). Once the starting p^*_{cm} is known, subsequent r_{c0} is defined with respect to the inertial origin for any further configuration as shown below:

$$r_{c0} = p^*_{cm} - \frac{1}{m_T}\sum_{i=1}^{n+1}\sum_{j=1}^{n+1} m_j\, r_{ci} \qquad (14)$$

where p^*_{cm} = initialised barycentric location, m_T = total mass of all links including spacecraft mount, r_{ci} = link vector from joint $i-1$ to link i centre of mass, m_j = mass of link j, n = number of manipulator links.

For this study, the problem is contrarywise and different. Here, the goal is to ensure that r_{c0} is kept adjustable, such that the center of mass of the spacecraft remains invariant as much as possible. For instance, when there is perturbation or any kind of disturbance, and r_{c0} has moved from the desired position, we could use the movement of robotic arm to adjust it back to the desired position, so as to keep the spacecraft's center of mass invariant. Since the initial position (r_{c0} vector) of the spacecraft would be known before any perturbation, a

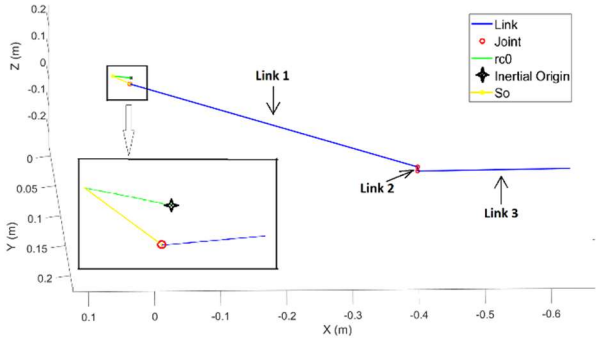

Fig. 3. Simulation of single space robotic interferometric platform.

mapping algorithm has been developed, such that, given the new position vector of r_{c0} of the spacecraft after an effect of perturbation, it is possible to map out the robotic joint-based solution required by the manipulator to return the spacecraft to its initial center of mass by adjusting r_{c0} back to its initial vector position. If this could be achieved to submicron accuracy, it means the spacecraft center of mass can be kept invariant to a very high precision, as required for interferometric constellation. As shown in equation (14), under robotic analysis, r_{c0} is only deduced from the configuration maneuver of the arm, where p^*_{cm} has to be calculated at first (with r_{c0} initialized as zero). Then, subsequent r_{c0} are calculated as the arm moves. Perturbation do not account for such; the whole spacecraft is perturbed with no correlation to the movement of the robotic arm (no correlation with the inertial space). Since r_{c0} is a position vector in 3-D, there are three known quantities of the vector in inertial space. To determine the post-perturbation p^*_{cm} position vector corresponding to the r_{c0}, a minimum of three robotic joint angles will be required to determine this unknown - see equation (15). On the other hand, we do not know the joint angles that would have resulted from a normal maneuver of the robotic arm, if it was meant to be a normal or predefined motion. This was a perturbation; we do not know the resulting robotic joint angles at this post-perturbation position. An algorithm has been developed to map out the robotic joint angles that would have corresponded to the r_{c0} of the perturbed state, if the robotic arms were to have had a predefined motion or normal maneuver. It was started by initializing the post-perturbation joint angles of at least three arms/links to zero. For the case of our simulation, the PUMA 560/600 was adopted, which has six joint angles. The first three joints angles were initialized as zero, while the last three joint angles from the wrist were taken simply as same as the terrestrial manipulation – this formulation has been established earlier [10]. The simulation started by assuming the space manipulator to be in the stowed position (before any perturbation), and p^*_{cm} was first calculated with respect to an inertial origin – see equation

(7), r_{c0} defined as zero. Then the space manipulator arm was moved to a randomly chosen position of [0.015, 0.015, 0.015] m with respect to the inertial origin, and the r_{c0} was calculated for this configuration according to equation (14). This was used to simulate the effect of perturbation, change in r_{c0} from [0, 0, 0] at the initial stowed state to some randomly chosen r_{c0} for the perturbed state. This completes the simulation of perturbation; now the problem is adjusting the r_{c0} back to its initial state.

Before the adjustment procedure, at first, a simple algorithm was written to determine the first three joint angles of the space manipulator in inertial space as at the time the p_{cm}^{*} was calculated in relation to the initialized r_{c0} of [0, 0, 0] - before perturbation. This simple algorithm follows as below:

R_iL_i is first calculated with respect to each link joint (i), in accordance to equation (8), also see reference [10]. This R_iL_i was calculated with these first three joint angles $x^u(1)$, $x^u(2)$, and $x^u(3)$ initialized as zeros at first, and joint angles for links 4, 5, and 6 of the manipulator taken as that of the initial terrestrial robot as established earlier [10]. A solver was used to solve the system of non-linear equation (derived as below) after R_iL_i has been initialized with the above stated joint angles:

$$\begin{aligned} x^u(1) &= p_{cm}^{*}(i) - \left(1 - \tfrac{m_0}{m_T}\right) s_0(i) - R_iL_i(:,:,i) - r_{c0}(i,:,u) \\ x^u(2) &= p_{cm}^{*}(j) - (1 - \tfrac{m_0}{m_T}) s_0(j) - R_iL_i(:,:,j) - r_{c0}(j,:,u) \\ x^u(3) &= p_{cm}^{*}(k) - \left(1 - \tfrac{m_0}{m_T}\right) s_0(k) - R_iL_i(:,:,k) - r_{c0}(k,:,u) \end{aligned} \quad (15)$$

Here, $r_{c0}(i,:,u)$ means $''i''$ vector of r_{c0} at the initial **u**nperturbed state denoted with $''u''$; meaning spacecraft (telescope) at initial launched position in inertial space before any maneuver or perturbation. Vector position in 3-D is represented by the $i-j-k$ in parentheses.

These equations were set as a Function $x^u(1{:}3)$ corresponding to the three joint-angles at initial state. The non-linear solver was implemented in iteration to map out the actual joint angles $x^u(1)$, $x^u(2)$ and $x^u(3)$ corresponding to the initially calculated p_{cm}^{*} (system center of mass) with respect to the defined inertial coordinates. This concludes the pre-perturbation simulation. Initial state r_{c0}, p_{cm}^{*}, and joint angles all calculated and defined.

A mapping algorithm was written to deduce the manipulators joint angles now at the perturbed state configuration (remember it won't be the stowed state joint angles anymore). The algorithm was developed to map out the robotic joint angles that would have corresponded to the r_{c0} of the perturbed state, if the robotic arms were to have had a predefined motion or normal maneuver.

This started by initializing the post-perturbation joint angles of the first three links to zero. For the PUMA manipulator, the first three joints angles are initialized as zero, while the last three joint angles from the wrist were taken as same as the terrestrial manipulator as previously mentioned [10]. The joint angles were represented by $x^p(1)$, $x^p(2)$ and $x^p(3)$ for the **p**erturbed state. Then the non-linear solver was implemented as described above in equation (15), but note that in this case, r_{c0} is assumed random and the exact position of the spacecraft center of mass (p_{cm}^{*}) is not initially known in the perturbed state. A loop was programmed to account for this as below: R_iL_i in the perturbed state was calculated with initialized zero joint angles $x^p(1)$, $x^p(2)$ and $x^p(3)$ Then implement

$$\begin{aligned} p_{cm}^{*} &= zeros(3,1) + (1 - \frac{m_0}{m_T}) s_0 + \sum R_iL_i + \dots \\ &\left(\frac{m_{n+1}}{m_T}\right) R_{n+1} r_{n+1}; \end{aligned} \quad (16)$$

The above p_{cm}^{*} here now is the system center of mass in the perturbed state relative to the inertial coordinate, but the r_{c0} is initialized as zeros(3,1) just to get the computational loop started. The actual p_{cm}^{*} will be mapped out from the loop for the solution of what the joint angles will be to match this p_{cm}^{*} when r_{c0} takes the value of the perturbed state.

7B. Simulation - Constellation Platform

For the purpose of interferometric imaging as described in section 3, a constellation of five free-flying spacecraft (telescopes) flying in formation as an astronomical interferometer was designed. The five spacecraft will act as chasers while there would be a target spacecraft acting as the beam combiner of the constellation to generate interferometric imaging. This simulation could be deployed to directly detect Earth-like planets orbiting nearby stars and possibly search for evidence of life on these planets. Interferometric method as presented here offers extremely high-resolution imaging, because each interferometric platform can be maintained stable to submicron accuracy by keeping the r_{c0} adjustable to the initial set position. The relative distance or separation between two neighboring spacecrafts is affected by the change in r_{c0} of either of the spacecraft during perturbation. The correction algorithm works in such a way that each spacecraft could be able to detect a change or shift in its r_{c0} and the manipulator is able to quickly respond to that change, adjusting it back to the desired set position. The same scenario is obtained by the neighboring spacecraft's r_{c0} experiencing any change or

shift, and as such, the relative distance between them is always kept as invariant as possible.

The mapping procedure was implemented in iterative computational loop using the Levenberg–Marquardt algorithm for the solver [21, 22] while making sure the trust-region size is adjusted accordingly at each iteration, with a tolerance value up to the order of 1e-9. With this, the robotic joint angles at the perturbed state can be successfully mapped out for the solution required for the p^*_{cm} and the r_{c0} to be satisfied at the specified perturbation state, up to submicron accuracy.

These perturbed state robotic joint angles are the required parameters to achieve the adjustment of r_{c0} back to what it was at the initial spacecraft center of mass which we wanted to maintain invariant. The robotic manipulator is then operated by performing joint-level trajectory motion (using the joint angles) from the perturbed state to the initial state.

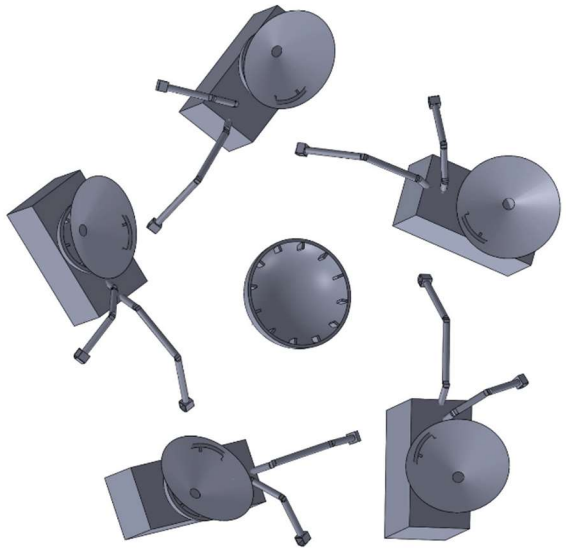

Fig. 4. Representation of four space robotic interferometric platforms in formation flying around the cantered beam combiner.

Each interferometric platform represents a spacecraft bus mount to which one or more manipulators are mounted as depicted in Figure 4. For the purpose of simulation, two different sizes of PUMA 560/600 manipulator configuration were considered. One was the original size of the manipulator, and the other was a smaller model of the manipulator, which was scaled down by an order (ratio) of 4. The original larger size was used simply for better visual representation as shown in Figure 5. For the purpose of real-life deployment, the smaller size manipulator would be ideal. It was evident from the simulation that smaller size manipulator allows for larger range of joint angle movement for an infinitely small r_{c0} adjustment, giving room for higher order accuracy. With the large arm manipulator, it would be required to move very small joint angles to correct the change in r_{c0}, resulting in lower order accuracy because the joint angle movement range is quite small. It is also possible that there are fewer motors available to provide such minimal angular movement. The space robot's design needs to be able to accommodate sizeable angular rotation that can be readily attainable by most commercial motors deployed at the joints. Although both large and small manipulators will be mounted unto the spacecraft, the magnitude of perturbation in Jupiter or Moon-L2 for instance, are of quite small magnitude [5]. For such order of perturbation, there would be tiny fraction of change in the r_{c0}, it would require a small-sized manipulator to deploy its arm with large joint angle movement so as to correct the r_{c0} with high degree of accuracy.

The key to this approach is providing submicron/micron accuracies in the control of the relative positioning with respect to the barycentric centre of mass without using fuel [1]. The position relative to the barycentre (r_{c0}) is controlled by the configuration of the manipulator(s) as shown earlier in section 7A, equation (16). This may be generalized to multiple manipulators. This suite of onboard manipulators automatically adjusts their configuration to maintain the constellation as a virtual optical bench. With reference to the Rayleigh criterion, the angular resolution, θ, is given by $\theta = 1.22\frac{\lambda}{D}$, where λ is the wavelength and D is the diameter of the aperture (telescope).

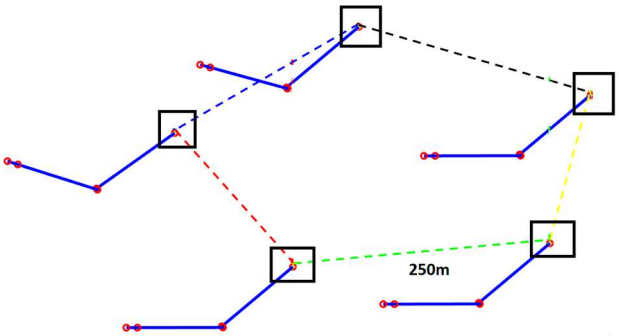

Fig. 5. MATLAB [24] simulation of five interferometric platforms, stable optical bench achieved against perturbation (larger manipulators)

With the implementation of near-infrared interferometric constellations, the free-flying telescopes combine into a "virtual optical bench" with diameter, D, of the utmost-separated apertures. With the apertures separated about

250 m apart, it would be possible to resolve an exoplanet with an angular diameter of up to 1 milliarcsecond – as the case for Alpha Centauri C (Proxima Centauri). The developed mapping algorithm demonstrates the relationship between the robotic manipulators' configuration such that joint-level trajectories are deduced to move or re-position the arm, resulting in a successful approach to accurately control the relative position between the interferometric platforms. Most importantly, no fuel is expended except for the initial configuration maneuvers. This simulation provides a robotic constellation approach to achieving interferometric imaging of terrestrial extrasolar planets.

8. Conclusions

With the algorithms and simulations carried out, it is possible to accurately control the relative positioning of spacecraft bus with a mounted manipulator by inducing base reactions at the mounted platform owing to its arm motion. Depending on the magnitude of perturbation and the change in r_{c0}, the manipulator joint angles need a motor rotation of the appropriate range. For the control and adjustment of relative position occurring within 10e-6 Nm of disturbance torque as considered in this study, a joint rotation of at least 3º up to about 32º was calculated to be required within the scale of the small and large manipulators described. Appropriate motors are available and can be selected within this required range, ultimately relying on the magnitude of disturbance or perturbation under consideration. The possibility of building these manipulators provides for useful and diverse application as being currently explored in the field of space robotics. It has been shown in this study that the manipulator-mounted spacecraft could exist as a single one, while there could be multiple spacecraft in free-flying formation with one or more manipulators mounted. Such constellations have been demonstrated as a matter of research interest for interferometric imaging in space. The mounted manipulators are deployed to control the relative positioning of the spacecraft as optical bench in free-flying formation. This has shown a viable way to revive the ESA's Darwin project or the NASA's Terrestrial Planet Finder (TPF) project. Beyond that, this ground-breaking approach can also be of interesting application in on-orbit servicing with two spacecraft's relative positioning adequately controlled. Spacing and rendezvous can also be controlled with the aid of the manipulator arm movement as mounted on the spacecraft. In general terms, it can be concluded from this study that: for any space telescope, given a desired translational motion (or the base reactions required for that), a mapping algorithm has been developed to deduce the joint-level trajectory needed to move the robotic arm from its present position to the required position in cartesian-space, corresponding to the desired platform reaction. As demonstrated, this validation provides grounds for accurate control of the spacecraft position, resulting in stable optical bench for interferometric imaging. With this, other viable and daunting applications could also be explored.

Appendix - Proof of Concept for Relative Position Control

In this case study, the smaller PUMA-like manipulator was adopted for the space manipulator. The parameters of the manipulator at the initial (stowed) position are shown below as used in the simulation:

Table 1. D-H Table and Initial Configuration (***Smaller Manipulator***)

Joint	Variable(º)	α_i(º)	$a_i(m)$	$d_i(m)$
1	θ_1	-90	0	0
2	θ_2	0	0.1080	0.0373
3	θ_3	90	0	0
4	θ_4	-90	0	0.1083
5	θ_5	90	0	0
6	θ_6	0	0	0.0141

Table 2. D-H Table and Initial Configuration (***Larger Manipulator***)

Joint	Variable(º)	α_i(º)	$a_i(m)$	$d_i(m)$
1	θ_1	-90	0	0
2	θ_2	0	0.432	0.1492
3	θ_3	90	0	0
4	θ_4	-90	0	0.4332
5	θ_5	90	0	0
6	θ_6	0	0	0.0564

The initial joint angles used for stowed position were θ_1 = -90º, θ_2 = -90º, θ_3 = 90º, while $\theta_4 = \theta_5 = \theta_6 = 0$. The parameters of the inertia moments (I_{cm}) were also chosen as used in the MATLAB code accordingly [23]. For the kinematic chain and the link masses, the following physical properties have been chosen [10]:

Table 3. Physical Properties of Manipulator and Spacecraft (***Smaller Manipulator***)

Kinematic Chain	Mass(kg)
Link 0 (spacecraft bus)	250
Link 1 (manipulator shoulder)	2
Link 2	1.5
Link 3 (manipulator elbow)	1.5
Link 4	0
Link 5 (manipulator wrist)	3
Link 6 (manipulator end-effector)	2
Link 7 (payload)	0

Table 4. Physical Properties of Manipulator and Spacecraft (***Larger Manipulator***)

Kinematic Chain	Mass(kg)
Link 0 (spacecraft bus)	250
Link 1 (manipulator shoulder)	8
Link 2	6
Link 3 (manipulator elbow)	6
Link 4	0
Link 5 (manipulator wrist)	12
Link 6 (manipulator end-effector)	8
Link 7 (payload)	0

For the kinematic solution, the procedure discussed and presented in Section 4 (Kinematic Analysis of Space-based Manipulator) was implemented for the ***smaller*** space manipulator. The position kinematic with respect to the inertial space as described in equation (10) was implemented in MATLAB. At first, the simulation of the manipulator was implemented in the terrestrial case with the specified D-H parameters. The forward kinematics of the manipulator in terrestrial-based application was calculated and the position of the end effector determined. To make sure and verify that the code was working correctly, the inverse kinematics was then calculated for the resulting position using the kinematic configuration of the manipulator, in an attempt to recalculate back the initial joint angle of the manipulator. It was confirmed that the inverse kinematics resulted back into the exact joint angles the manipulator was initialized with (prior to the forward kinematics calculation). The key to the space application approach is to replace the terrestrial parameters of a_i and d_i with the spaced-based equivalence [10], taking into account the lumped kinematic parameters as described in Section 4.

This procedure was implemented in the MATLAB code. Having implemented the space-based kinematic/lumped parameters, the position of the end-effector in space with respect to the inertial base (p^*) is then calculated through the forward kinematics; the corresponding space-based joint angles for this were calculated through the inverse kinematics. This concludes the space-based forward position and inverse joint angles at the initial position of the manipulator. It is to be noted that the manipulator's arm position is considered only to the wrist level in the cartesian space position, as it is customarily done [10], and the manipulator cartesian position is represented by $Parm$ at this level. In the MATLAB code, also the parameters $Parm$ and $R_i\lambda_i$ were calculated and implemented. $Parm$ was calculated to be $(0.2105, 0, 0.036)$ for the space manipulator. The s_0 was chosen arbitrarily as $[0.00075; 0.0015; -0.002]$ in metres, an assumption made for the position vector of the manipulator base with respect to the spacecraft body center of mass – this would have to be given in reality. Now to simulate trajectory, a desired end point (final position) was specified for the space manipulator; this was represented by $P_{end} = [0.015; 0.015; 0.015]$ in the MATLAB code. A cartesian trajectory "knot points" generation was carried out using five segment trajectories, and a 6-point knot points were generated between the initial position of the manipulator in space and the given desired final position. The six knot points are represented in cartesian space (up to the wrist) level, and the corresponding joint angles $(\theta_1 - \theta_6)$ were calculated (for each knot point) by the inverse kinematics.

The inverse kinematics joint angles for the knot points were obtained and Jacobians were also obtained for the required resolved motion control formulation. For the resolved motion control, the Bang-Bang approach was adopted for the velocity and acceleration rate profile. Generation of joint-level trajectory in between the knot points was carried out with the so-called patching procedure, patching the knot points together using five segments cubic spline polynomial [12]. With this, it was possible to fully describe the forward trajectory motion of the space manipulator arm, simulating the movement of the arm from the initial position to the specified desired position. Figure 5 shows what is seen in the simulation (five interferometric platforms), with manipulators shown up to the wrist. Lastly, the Newton-Euler dynamic formulation was carried out for the calculation of joint torques at each link. The procedure follows the steps and equations described in Section 6.

For the purpose of relative positioning application, the base-referenced torque is required to be calculated and the resulting reactions at the base of the spacecraft owing to the movement of the mounted manipulator arm. This trivially follows the same Newton-Euler dynamics as presented but with the simulation done with respect to inertial base. The program can be easily modified, and every link-referenced equation is transformed or returned as base-referenced [12]. The relationship to calculate the moments and forces on the spacecraft at the manipulator base $(x_0 y_0 z_0)$ with respect to inertial coordinates has been derived and given as [10]:

$$N_0 = N_T + [m_T(p^*_{cm} - r_{c0}) - (m_T - m_0)s_0] \times F_T/m_T$$

where

$$F_T = \sum_{i=1}^{n+1} F_{ci} = \sum_{i=1}^{n+1} m_i \dot{v}_{ci} \quad \text{(total force at base)}$$

$$N_T = \sum_{i=1}^{n+1} N_{ci} = \sum_{i=1}^{n+1} I_i \dot{\omega}_i + \omega_i \times I_i\omega_i \quad \text{(moment)}$$

F_{ci} is the total force on the link i center of mass, N_{ci} is the total moment about the link i center of mass, while $\dot{v}_{ci}$ is the linear acceleration of the link i center of mass. The resulting summed torque at the base of the spacecraft, as the arm moved along the knot points can be calculated, with an assumption made for the position vector of the manipulator base with respect to the spacecraft body center of mass (s_0) – this would have to be given in reality for accurate simulation.

References

[1] Ellery, A. An engineering approach to the dynamic control of space robotic on-orbit servicers, Proc. Instn Mech. Engrs, 2004, Vol. 218 Part G: J. Aerospace Engineering 218, 79-98.

[2] Estalella, Robert. Maximum angular size sensitivity of an interferometer, October 2008.

[3] Aerospace Guide, http://www.aerospaceguide.net/proxima-centauri.html

[4] Glass, I. S. The Discovery of the Nearest Star. Publication of African Sky, Vol. 11, p.39, July 2007.

[5] Shrivastava, S. and Modi, V. Satellite attitude dynamics and control in the presence of environmental torques—a brief survey. J. Guidance, 1983, 6(6), 461–471.

[6] Lindberg, R., Longman, R. and Zedd, M. Kinematics and reaction moment compensation for the spaceborne elbow manipulator. AIAA 86-0250, 1986.

[7] Longman, R., Lindberg, R. and Zedd, M. Satellite-mounted robot manipulators—new kinematics and reaction compensation. Int. J. Robotics Res., 1987, 6(3), 87–103.

[8] Vafa, Z. and Dubowsky, S. On dynamics of manipulators in space using the virtual manipulator approach. In Proceedings of IEEE International Conference on Robotics and Automation, 1987, pp. 579–585.

[9] Vafa, Z. and Dubowsky, S. Kinematics and dynamics of space manipulators: the virtual manipulator approach. Int. J. Robotics Res., 1990, 9(4), 852–872.

[10] Ellery, A. An Introduction to Space Robotics, Praxis– Springer Series on Astronomy and Space Sciences, 2000 (Praxis Publishers).

[11] Paul, R. Robot manipulators: mathematics, programming and control (MIT Press, Cambridge, Massachusetts).

[12] Fu, K., Gonzalez, R. and Lee, C. Robotics: Control, Sensing, Vision and Intelligence, 1987 (McGraw-Hill, Singapore).

[13] Denavit, J. and Hartenburg, R. Kinematics notation for lower pair mechanisms based on matrices. Trans. ASME, J. Appl. Mechanics, 1955, 77, 215–221.

[14] Ellery, A. Systems design and control of a free-flying space robotic manipulator system (ATLAS) for in-orbit servicing operations. PhD thesis, Cranfield Institute of Technology (now Cranfield University), 1996.

[15] Ellery, A. Resolved motion control of space manipulators. In Proceedings of 45th IAF Congress, Tel Aviv, Israel, 1994, ST 94-W2-574.

[16] Whitney, D. Mathematics of coordinated control of prosthetic arms and manipulators. Trans. ASME, Dynamic Syst. Measmt and Control, 1972, 122, 303–309.

[17] Luh, J., Walker, M. and Paul, R. Resolved acceleration control of mechanical manipulators. IEEE Trans. Autom. Control, 1980, 25(3), 236–241.

[18] Moya, M. and Seraji, H. Robot control systems: a survey. Robotics and Autonom. Syst., 1987, 3, 329–351.

[19] Kane, T. and Levinson, D. Formulation of equations of motion for complex spacecraft. J. Guidance and Control, 1983, 6(2), 99–122.

[20] Nagashima, F. and Nakaruma, Y. Efficient computation scheme for the kinematics and inverse dynamics of a satellite-based manipulator. In Proceedings of IEEE International Conference on Robotics and Automation, 1992, pp. 905–912.

[21] Levenberg, Kenneth (1944). "A Method for the Solution of Certain Non-Linear Problems in Least Squares". Quarterly of Applied Mathematics. 2 (2): 164–168.

[22] Marquardt, Donald (1963). "An Algorithm for Least-Squares Estimation of Nonlinear Parameters". SIAM Journal on Applied Mathematics. 11 (2): 431–441.

[23] Armstrong, B., Khatib O., Burdick J. The explicit dynamic model and inertial parameters of the PUMA 560 arm. Proceedings of 1986 IEEE international conference.

[24] MathWorks, “MATLAB,” 2019. The MathWorks Natick, MA.